

Analytic treatment of a linear electric field
frequency shift induced in confined gases by a
magnetic field gradient: Implications for
neutron electric dipole moment experiments

S.K. Lamoreaux
Los Alamos National Laboratory
P-23
Los Alamos, NM

R. Golub
North Carolina State University
Raleigh, NC
(present address, Hahn Meitner Institut, Berlin, Germany)

February 9, 2020

Abstract

The search for particle electric dipole moments (edm) is one of the best places to look for physics beyond the standard model because the size of time reversal violation predicted by the standard model is incompatible with present ideas concerning the creation of the Baryon-Antibaryon asymmetry. As the sensitivity of these edm searches increases more subtle systematic effects become important. We develop a general analytical approach to describe a systematic effect recently observed in an electric dipole moment experiment using stored particles [2]. Our approach is based on the relationship between the systematic frequency shift and the velocity autocorrelation function of the resonating particles. Our results, when applied to well-known limiting forms of the correlation function, are in good agreement with both the limiting cases studied in recent work that employed a numerical/heuristic analysis. Our general approach explains some of the surprising results observed in that work and clarifies several points.

Contents

1	Introduction	2
1.1	Brief description of the effect	4
2	Wall collisions	5
3	Frequency shift due to fluctuating fields in the x-y plane	6
3.1	Density matrix approach to the problem	6
3.2	Numerical estimations of the correlation functions	10
3.3	General solution for a radial magnetic field plus $v \times E$	11
3.3.1	Example: Particle in circular orbit	13
4	Influence of collisions on the E-proportional frequency shift	13
4.1	Short correlation times ($\omega_r \ll \omega_o$)	14
4.2	Diffusion theory calculation of the long time behavior of the velocity correlation function. Frequency shifts for ($\omega_r \gg \omega_o$) .	15
4.2.1	Green's function for the diffusion equation in cylindrical geometry	15
4.2.2	Velocity autocorrelation function	17
4.2.3	Frequency shift in the diffusion approximation (cylindrical geometry)	17
4.2.4	Frequency shift in the diffusion approximation (rectangular geometry)	18
4.3	Application: ^3He Comagnetometer	19
5	Conclusion	20
6	Acknowledgements	20
7	Appendix: Matrix algebra of spherical Pauli matrices	20
8	Figures	22

1 Introduction

The search for an electric dipole moment (EDM) of the neutron is perhaps unique in modern physics in that experimental work on this subject has been

going on more or less continuously for over 50 years. In that period the experimental sensitivity has increased by more than a factor of 10^6 without an EDM ever being observed. The reason for this apparently obsessive behavior by a small group of dedicated physicists is that the observation of a non-zero neutron EDM would be evidence of time reversal violation and for physics beyond the so-called Standard Model of electroweak interactions. An essential point is that the Standard Model predictions of the magnitude of time reversal violation are inconsistent with our ideas of the formation of the universe; namely the production of the presently observed matter - anti-matter asymmetry requires time reversal violation many orders of magnitude greater than that predicted by the Standard Model.

In this type of experiment (null experiment) the control of systematic errors is of great significance. While the switch of experimental technique from beam experiments to experiments using stored Ultra-cold neutrons (UCN) has eliminated many of the sources of systematic error associated with the beam technique, the gain in sensitivity brought by the new UCN technique means that the experiments are sensitive to a new range of systematic errors. One of the most serious of these is associated with the interaction of gradients of the ever-present constant magnetic field with the well known motional magnetic field $\left(\frac{\vec{v}}{c} \times \vec{E}\right)$. As the particles move in the apparatus, these fields, as seen by the particles, will be time dependent. This effect was first pointed out by Commins [1] and explained in terms of the geometrical phase concept. A more general description is in terms of the Bloch-Siegert shift of magnetic resonance frequencies due to the time dependent fields mentioned above [2],[3].

The effect was apparently empirically identified in the ILL Hg comagnetometer EDM experiment and recently Pendlebury et al [2] have given a very detailed discussion of it, including intuitive models and analytical calculations for certain cases, the relation between and regions of applicability of the geometric phase and Bloch-Siegert models, numerical simulations and experimental verification of the most significant features. However this pioneering work has left certain questions unanswered. In particular the understanding of effects of collisions on the systematic frequency shifts remains incomplete.

In this work we attempt to clarify several points concerning the influence of particle collisions. We explain the reason that in contrast to gas collisions, collisions with the walls apparently have no effect on the magnitude of the systematic frequency shifts. We then show that the frequency shift is related to the velocity autocorrelation function of the resonating particles. Our solution, when applied to well known limiting forms of the correlation function,

gives results in agreement with those obtained numerically in [2]. McGregor has taken a similar approach to the problem of relaxation due to static field gradients [4], whereas the approach taken by Cates et al to the problem of static field gradients [5] and gradients combined with oscillating perturbing fields [6] is somewhat different than ours.

1.1 Brief description of the effect

Consider a case where, in a storage experiment, there is a radial magnetic field due to a magnetic field gradient in the z direction (B_0 , the quantization axis, and the electric field E are along z). Now consider roughly circular orbits, due to reflection around the bottle at a constant angle, in the $x - y$ plane with radius approximately the bottle radius R . The wall collisions occur at a frequency $1/\tau_c$ while the orbital frequency is $\omega_r = 2\alpha/\tau_c$ where α is the incidence angle relative to the surface. We can transform into a rotating frame at ω_r (note that this is not the Schwinger rotating frame that eliminates B_0) so that the problem is quasi-static [3].

The radial field, with the barrel gradient plus $v \times E$ field, is

$$B_R = B_r \pm B_E = aR \pm \frac{\omega_r R E}{c}$$

where $B_r(r) = (r/2) \partial B_z / \partial z = ar$ is the radial field due to the axial gradient, and $\pm B_E = r\omega_r E/c$ is the radially directed $v \times E$ field and the \pm refer to the rotation direction.

In the rotating frame,

$$B^2 = (B_0 - \omega_r/\gamma)^2 + (B_R)^2$$

where γ is the gyromagnetic ratio. Expanding in the limit where $B_R \ll B_0$ with transformation back to the lab frame we find

$$B = B_0 + \frac{1}{2} \frac{(aR - \omega_r R E/c)^2}{B_0 - \omega_r/\gamma} = B_0 - \frac{(aR^2 \omega_r E/c)}{B_0 - \omega_r/\gamma}$$

keeping only terms linear in B_E . Averaging over rotation direction (e.g., the sign of ω_r , the net effect of the gradient field combined with a $v \times E$ yields a systematic (magnetic field) shift of

$$\delta\omega = \gamma\delta B = -\frac{\gamma^2 a v^2 E}{c(\omega_0^2 - \omega_r^2)} \quad (1)$$

equivalent to Eq. (18) of [2]. Taking the limit $\omega_r/\gamma \ll B_0$ we have

$$\delta B = -\frac{aR^2 \omega_r^2 E}{\gamma c B_0^2}, \quad \delta\omega = -\frac{aR^2 \omega_r^2 E}{c B_0^2} \quad (2)$$

where which would seem to set the scale of the effect and is equivalent to Eq. (19) of [2]. In this limit, the frequency shift does not depend on γ , implying that it is the result of a geometric effect.

In the other limit, where the rotation frequency is much faster than the Larmor frequency, we similarly find that

$$\delta B = \gamma a R^2 E / c, \quad \delta \omega = \gamma^2 a R^2 E / c \quad (3)$$

which is independent of the motional frequency ω_r of opposite sign from the previous limit and equivalent to Eq. (21) or [2].

2 Wall collisions

One of the surprising, but unexplained results of [2] was that according to the numerical simulations, wall collisions had no influence on the magnitude of the frequency shifts while gas collisions could eliminate the frequency shifts completely if their rate is high enough. We now show that the reason for this is that the wall collisions are never fast enough to influence the systematic (proportional to \vec{E}) frequency shifts.

For a particles in a cylindrical vessel following a trajectory along a chord subtending an angle 2α , the time between collisions is

$$\tau_c = \frac{2R}{v} \sin \alpha \quad (4)$$

and the effective field rotation frequency is given by

$$\omega_r = 2\alpha / \tau_c = \frac{\alpha v}{R \sin \alpha} \quad (5)$$

Considering first the case when $\omega_r \gg \omega_o$ ([2] Fig. 10) the systematic frequency shift was found to be suppressed by the factor η

$$\eta = \frac{1}{1 + \beta^2}$$

$$\beta = \frac{2R^2 \omega_o}{\pi v^2 \tau_c}$$

For significant suppression we need $\beta \gtrsim 1$

$$\frac{2R^2 \omega_o}{\pi v^2 \tau_c} = \frac{R \omega_o}{\pi v \sin \alpha} \gtrsim 1 \quad (6)$$

$$\sin \alpha \lesssim \frac{R \omega_o}{\pi v} = \frac{25 \times 2 \cdot 7}{10^4} \sim \frac{1}{30}$$

for representative conditions in fig. 10. ($R = 25, B_o = 1\mu T, v = 10^4 cm/sec$).

The probability of a given value of α is given in Eq. (B1) of [2] as

$$P(\alpha)d\alpha = \frac{4}{\pi} \sin^2 \alpha d\alpha \quad (7)$$

$$P(\alpha \leq \varepsilon) \sim \varepsilon^3$$

so that the wall collisions would only be expected to be effective for a vanishingly small fraction of the trajectories.

Turning now to the case $\omega_r \ll \omega_o$ (Fig. 12 of [2]) we have as the condition that the suppression be effective:

$$\beta = \frac{1}{\omega_o \tau_c} \geq 1$$

$$\frac{1}{\omega_o} \gtrsim \frac{2R}{v} \sin \alpha$$

$$\sin \alpha \leq \frac{v}{2R\omega_o} = \frac{200}{2 \cdot 25 \cdot 200} = \frac{1}{50}$$

for conditions typical of [2] Fig. 12 ($v = 200 cm/sec, B_o = 1\mu T$).

Thus the wall collisions rate is never high enough to significantly effect the magnitude of the frequency shift. The wall collisions do, however, broaden and shift the resonances discussed in [2] (see below).

3 Frequency shift due to fluctuating fields in the x-y plane

3.1 Density matrix approach to the problem

The issues of the effects of a weak fluctuating potential on the evolution of the density matrix have been well-addressed in the literature. However, these treatments generally assume that the perturbing potential has a short correlation time, and certain assumptions regarding averaging are not applicable to our problem. The effect of a static electric field E by itself was treated in [7] where the E^2 effect was related to the correlation time, and requirements on the field reversal accuracy were discussed.

So we therefore start from the beginning, following [8] (p. 276).

The radial gradient and $v \times E$ fields can be treated as weak fluctuating perturbing fields $B_{x,y}(t)$ in the $x - y$ plane, with a constant B_0 applied along

z. The perturbing fields $B'_{x,y}(t)$ can be written as

$$B'_x(t) = B_x(t) - \langle B_x(t) \rangle; \quad B'_y(t) = B_y(t) + \langle B_y(t) \rangle \quad (8)$$

where $\langle \dots \rangle$ represents a time average of $B_{x,y}(t)$. The constant component of the perturbing field are added to B_0 ,

$$B'_0 = \sqrt{(B_0)^2 + \langle B_x(t) \rangle^2 + \langle B_y(t) \rangle^2} \quad (9)$$

leaving the perturbing fields with averages of zero. We define

$$\omega_0 = \gamma B'_0; \quad \omega_{x,y}(t) = \gamma B'_{x,y}(t). \quad (10)$$

The Hamiltonian is thus

$$H = -\frac{\omega_0}{2}\sigma_z - \frac{\omega_x}{2}\sigma_x - \frac{\omega_y}{2}\sigma_y = H_0 + H_1(t). \quad (11)$$

Defining

$$2b = \omega_x + i\omega_y; \quad 2b^* = \omega_x - i\omega_y \quad (12)$$

the perturbing Hamiltonian can be rewritten as

$$H_1(t) = b\sigma_+ + b^*\sigma_- \quad (13)$$

where σ_{\pm} are defined in the appendix, and it is understood that b is intrinsically time-dependent. Furthermore, the density matrix can be expanded in the spherical Pauli basis,

$$\rho = 1 + \rho_{1,0}\sigma_z + \rho_{1,1}\sigma_+ + \rho_{1,-1}\sigma_- \quad (14)$$

where $\rho_{11} = \rho_{1,-1}^*$.

The time evolution of the density matrix is

$$\frac{d\rho}{dt} = -i[H_0 + H_1(t), \rho]. \quad (15)$$

The explicit dependence on the constant H_0 can be eliminated by transforming to the rotating frame (also called the interaction representation), with

$$H_1(t) \rightarrow e^{iH_0t} H_1(t) e^{-iH_0t}; \quad \rho \rightarrow e^{iH_0t} \rho e^{-iH_0t} \quad (16)$$

where

$$e^{iH_0t} = \begin{pmatrix} e^{-i\omega_0t/2} & 0 \\ 0 & e^{i\omega_0t/2} \end{pmatrix} \quad (17)$$

We henceforth will work in the rotating frame, with

$$H_1(t) = e^{-i\omega_0 t} b \sigma_+ + e^{i\omega_0 t} b^* \sigma_-. \quad (18)$$

The time evolution of the density matrix in the rotating frame is

$$\frac{d\rho}{dt} = -i[H_1(t), \rho] \quad (19)$$

which can be integrated by successive approximations to

$$\begin{aligned} \rho(t) = & \rho(0) - i \int_0^t [H_1(t'), \rho(0)] dt' \\ & - \int_0^t dt' \int_0^{t'} dt'' [H_1(t'), [H_1(t''), \rho(0)]]. \end{aligned} \quad (20)$$

We are interested in the relaxation rates and frequency shifts due to the perturbing fields, which can be found through the time derivative of ρ , which by introducing a new variable $\tau = t - t''$, is

$$\frac{d\rho}{dt} = -i[H_1(t), \rho(0)] - \int_0^t d\tau [H_1(t), [H_1(t - \tau), \rho(0)]]. \quad (21)$$

The first term on the r.h.s has an ensemble average of zero; furthermore, there is no correlation between ρ and the fluctuating Hamiltonian (e.g., phases of the neutrons have no explicit spatial dependence, and $H_1(t)$ is different for every neutron in the system). In addition, if we assume the perturbation is weak, $\rho(0)$ can be replaced by $\rho(t)$ which introduces errors below second order.

We then have

$$\frac{d\rho}{dt} = - \int_0^t d\tau [H_1(t), [H_1(t - \tau), \rho(t)]] \equiv \Gamma \rho(t) \quad (22)$$

where Γ is the "relaxation matrix", the real parts of which describe decays of coherence, and the imaginary parts of the off-diagonal elements describe frequency shifts.

Using the relations in Appendix A together with the expansion of the density matrix Eq. (14), the time-derivative of ρ , correct to second-order and neglecting $2\omega_0$ terms, is

$$\dot{\rho}_{1,-1} = -\rho_{1,-1} \int_0^t 2e^{i\omega_0 \tau} b^* b' d\tau \quad (23)$$

$$\dot{\rho}_{1,1} = -\rho_{1,1} \int_0^t 2e^{-i\omega_0 \tau} b b'^* d\tau \quad (24)$$

$$\dot{\rho}_{1,0} = -\rho_{1,0} \int_0^t 4\text{Re} [e^{i\omega_0 t} b'^* b] d\tau \quad (25)$$

where

$$2b = \omega_x(t) + i\omega_y(t); \quad 2b' = \omega_x(t - \tau) + i\omega_y(t - \tau). \quad (26)$$

These equations describe both frequency shifts and relaxations of the density matrix. We are at present most interested in frequency shift, which is given by the difference in the off-diagonal components of Γ . Expanding b and b' we find

$$\begin{aligned} \delta\omega(t) = & -\frac{1}{2} \int_0^t [\cos \omega_0\tau (\omega_x(t)\omega_y(t - \tau) - \omega_x(t - \tau)\omega_y(t)) \\ & + \sin \omega_0\tau (\omega_x(t)\omega_x(t - \tau) + \omega_y(t)\omega_y(t - \tau))] d\tau. \end{aligned} \quad (27)$$

This is the general solution for the frequency shift given an arbitrary perturbing field. An ensemble average must be taken.

The identical result is obtained with appropriate ($\omega_{x,y}, \delta\omega \ll \omega_o$) approximations from the Bloch equation in the form given in Eqs. (46) and (47) of [2]. This is quite interesting given the different assumptions made in the two approaches.

Now $\omega_x = ax + bv_y, \omega_y = ay - bv_x$ where

$$a = \frac{\gamma}{2} \frac{\partial B_z}{\partial z} \quad (28)$$

$$b = \gamma \frac{E}{c} \quad (29)$$

with γ the gyromagnetic ratio and it is clear that only the cross-terms $\omega_x\omega_y$ will result in a non-zero linear E ($\propto b$) shift,

$$\begin{aligned} \delta\omega = & -\frac{1}{2} \int_0^t d\tau (\cos \omega_o\tau) \{ \langle \omega_x(t)\omega_y(t - \tau) \rangle - \langle \omega_x(t - \tau)\omega_y(t) \rangle \} \\ = & \frac{ab}{2} \int_0^t d\tau (\cos \omega_o\tau) R(\tau) \end{aligned} \quad (30)$$

where

$$R(\tau) = \left\langle y(t)v_y(t - \tau) + x(t)v_x(t - \tau) - y(t - \tau)v_y(t) - x(t - \tau)v_x(t) \right\rangle \quad (31)$$

is the net correlation function, where $\langle \dots \rangle$ represents an ensemble and time average.

3.2 Numerical estimations of the correlation functions

The problem of the neutron EDM experiment with a ^{199}Hg comagnetometer subject to a time-varying $v \times E$ field in combination with a spatially-varying magnetic field is described in [2] and in the Introduction. We assume a cylindrical volume with radial field $\vec{B}(r) = a'r\hat{r}$. The electric field is constant everywhere and along the \hat{z} direction. Assuming a constant velocity v , the $v \times E$ field is then fluctuating in direction but of spatially uniform magnitude.

A numerical calculation of the correlation function was performed for the two-dimensional case (UCN or Hg at a fixed z , moving only in $x - y$ plane). This problem can be parameterized in terms of the time between collisions $\tau_c = \lambda/v$, where the mean free path between collisions is λ and the average velocity is v . For the numerical calculations, v is assumed constant. Time can be parameterized in dimensionless units, τ/τ_c . The correlation function was calculated by statistically choosing a propagation distance for a fixed velocity direction, and taking time steps of 0.025, after which a new random velocity direction was chosen. Various degrees of specularity, parameterized by $\Delta\theta$ for the statistical degree of angular change for reflection from the bottle surface, were considered.

Results of a two-dimensional Monte Carlo calculation are shown in Figure 1. Taking $\lambda = 1$ and fixed, we see the effect of wall collisions as the bottle radius approaches λ . We see in Fig. 1 that in all cases $R(\tau)$ initially increases linearly. The effect of the wall collisions when $R > \lambda$ is to limit the distance that the random walk can take, and this appears as an exponential decay in $R(\tau)$ at long times. This effect does not depend on the specularity of the wall collisions and is best seen as an effect on the whole ensemble of particles which can be described by classical diffusion theory. In this limit, the correlation function is well-described by

$$R(\tau) = (1 - e^{-\tau/\tau_c})e^{-\tau/T} \quad (32)$$

where, from analysis of the plots,

$$T \approx \frac{0.6R^2}{\lambda v}. \quad (33)$$

In the other limit, $R < \lambda$, $R(\tau)$ oscillates with frequency

$$\omega \approx \frac{2\pi v}{5.2R} \quad (34)$$

and

$$R(\tau) = e^{-\tau/T} \sin \omega\tau \quad (35)$$

where T depends on $\Delta\theta$, but is typically of order $2\pi/\omega$.

The frequency shift is determined by Eq. (30) and in the case of large R we find ($\tau_c \ll T$), using Eq. (33)

$$\delta\omega = \frac{abR^2}{T^2\omega_0^2 + 1} = \frac{abR^2}{1 + (0.6R^2\omega_0/v\lambda)^2}. \quad (36)$$

These results are in good agreement with [2], Fig. 10, for which $4/2\pi \approx 0.634$ replaces the factor 0.6 above and with equ. (75) below.

Additional insight can be gained by considering the effects of varying λ keeping R fixed, as shown in Fig. 2 for very small λ . In this limit, the horizontal axis is multiplied by λ/R to define time proportional to R/v . The correlation amplitude function is proportional to λv and the decaying exponential time constant is

$$T \propto \frac{R^2}{\lambda v}. \quad (37)$$

The time to reach the peak value is

$$\tau_0 \propto \lambda^2/Rv \quad (38)$$

which approaches zero as $R \rightarrow \infty$.

This limit is further discussed in Sec. 4.1, and the frequency shift in this case is in general agreement with Fig. 10 of [2].

The curves for large (relative to R) λ in figure 1 show damped oscillations whose damping depends on the angular spread of the wall collisions. This is a manifestation of the resonance behavior discussed in ref. [2] for the case of perfectly specular wall collisions. Here we see the damping to non-specular reflections. We do not discuss this further here as the main thrust of this paper is the reduction of the effect at higher collision rates.

3.3 General solution for a radial magnetic field plus $\mathbf{v} \times \mathbf{E}$

According to (30) the frequency shift is proportional to the Fourier transform of the correlation function $R(\tau)$, between (y, v_y) and (x, v_x) evaluated at the Larmor frequency, ω_0 . However this can be written in terms of the velocity autocorrelation function as follows:

$$\begin{aligned} y(t) &= y_o + \int_0^t v_y(t') dt' \\ y(t - \tau) &= y_o + \int_0^{t-\tau} v_y(t') dt' \end{aligned} \quad (39)$$

Since there are no correlations between y_o and v_y the y terms in (31) are

$$A = y(t)v_y(t - \tau) = \int_0^t \langle v_y(t') v_y(t - \tau) \rangle dt' \quad (40)$$

$$B = y(t - \tau)v_y(t) = \int_0^{t-\tau} \langle v_y(t') v_y(t) \rangle dt' \quad (41)$$

$$\begin{aligned} R_y(\tau) &= A - B = \\ &= \left(\int_0^t \langle v_y(t') v_y(t - \tau) \rangle dt' - \int_0^{t-\tau} \langle v_y(t') v_y(t) \rangle dt' \right) (ab) \end{aligned} \quad (42)$$

$$= \int_{\tau-t}^{\tau} dx \psi(x) - \int_{\tau}^t dx \psi(x) \quad (43)$$

where $\psi(x)$ is the velocity autocorrelation function and we used the fact that it is an even function of x . Repeating the same argument for the x axis we have

$$\begin{aligned} \psi(\tau) &= \langle v_y(t) v_y(t - \tau) + v_x(t) v_x(t - \tau) \rangle \\ &= \langle \vec{v}_{xy}(t) \cdot \vec{v}_{xy}(t - \tau) \rangle \end{aligned}$$

$$R(\tau) = \int_{\tau-t}^{\tau} dx \psi(x) - \int_{\tau}^t dx \psi(x) \quad (44)$$

$$= 2h(\tau) - h(t - \tau) - h(t) \quad (45)$$

$$= 2h(\tau) \quad (46)$$

$$h(\tau) = \int_0^{\tau} dx \psi(x) \quad (47)$$

and we consider only cases where $\psi(x) \rightarrow 0$ as $x \rightarrow \infty$ so that we can take the limit $t \rightarrow \infty$ in equ. (45) and we note that a constant term in R will not have any effect on (30) contributing only a term $\propto \delta(\omega_o) = 0$.

According to (30) we need the cos Fourier transform of $R(\tau)$. This will involve $1/\omega$ times the FT of $\psi(x)$ which in turn is proportional to ω^2 times the FT of the position correlation function as we shall see. Substituting (45) into (30) we have

$$\delta\omega = ab \int_0^t d\tau (\cos \omega_o \tau) h(\tau) \quad (48)$$

Writing the velocity correlation function as

$$\psi(t) = \int_{-\infty}^{\infty} \cos \omega t \psi(\omega) d\omega \quad (49)$$

we have

$$h(\tau) = \int_0^{\tau} \psi(t) dt = \int_{-\infty}^{\infty} \psi(\omega) \left(\frac{\sin \omega \tau - 1}{\omega} \right) d\omega \quad (50)$$

so that according to (48) the frequency shift is given by (dropping the time independent term)

$$\begin{aligned} \delta\omega &= ab \left[\int_0^t d\tau \cos \omega_o \tau \int_{-\infty}^{\infty} \psi(\omega) \frac{\sin \omega \tau}{\omega} d\omega \right] \\ \delta\omega &= -ab \int_{-\infty}^{\infty} \frac{\psi(\omega)}{(\omega_o^2 - \omega^2)} d\omega \end{aligned} \quad (51)$$

The equation (51) represents the general solution to our problem which is simply the single frequency B-S result (equ. 1, [2] Eq. (18)) summed over the frequency spectrum of the velocity autocorrelation function plus oscillating terms (omitted) that don't contribute as long as $\psi(x) \rightarrow 0$ as $x \rightarrow \infty$.

3.3.1 Example: Particle in circular orbit

For a particle in an hypothetical circular orbit with orbital frequency $\omega_r \neq \omega_o$ we have

$$\begin{aligned} \psi(\tau) &= v_{xy}^2 \cos \omega_r \tau \\ \psi(\omega) &= v_{xy}^2 \delta(\omega - \omega_r) \end{aligned} \quad (52)$$

and substituting in (51)

$$\begin{aligned} \delta\omega &= -ab \int_{-\infty}^{\infty} v_{xy}^2 \delta(\omega - \omega_r) \frac{1}{\omega_o^2 - \omega^2} d\omega + \text{oscillating terms} \\ &= -\frac{abv_{xy}^2}{\omega_o^2 - \omega_r^2} \end{aligned} \quad (53)$$

in agreement with (1 and Eq. (18) of [2]) and valid for the case when $(\omega_o - \omega_r) > \omega_{x,y}$.

4 Influence of collisions on the E-proportional frequency shift

Equation (51) represents the formal solution of the problem in all cases of interest here. Thus the frequency shift is determined entirely by the velocity auto-correlation function of the particles undergoing magnetic resonance.

This function has been the subject of intense experimental and theoretical study ([13, 14, 15]). In our case, involving macroscopic distances and times, it suffices to treat the motion classically. For relatively short times if the particles undergo collisions which are distributed according to a Poisson distribution with average time between collisions given by τ_c , the velocity correlation function is well known to be given by

$$\psi(t) = \langle v^2 \rangle e^{-t/\tau_c} \quad (54)$$

This form is known to be valid for relatively short times. According to Eq. (48) the frequency shift depends on the Fourier transform of the velocity correlation function evaluated at ω_o . So the short time behavior of $\psi(t)$ determines the high frequency behavior of $\psi(\omega)$, so the result using this form is expected to be valid in the case of large ω_o , i.e. $\omega_o \gg \omega_r$.

For longer times the velocity correlation function is well described by classical diffusion theory. Thus the long time behavior will determine the low frequency region of the velocity spectrum and the result will apply to the case $\omega_o \ll \omega_r$. In this region the result will depend on the size of the containing vessel as the dynamics of the diffusion process are influenced by the boundary conditions.

4.1 Short correlation times ($\omega_r \ll \omega_o$)

Using (54) we have

$$\psi(\omega) = \frac{1}{\pi} \langle v^2 \rangle \int_0^\infty \cos \omega t e^{-t/\tau} dt = \frac{1}{\pi} \langle v^2 \rangle \frac{1}{\tau (\omega^2 + \frac{1}{\tau^2})} \quad (55)$$

so that according to (51)

$$\delta\omega = -ab \int_{-\infty}^{\infty} \frac{\psi(\omega)}{(\omega_o^2 - \omega^2)} d\omega \quad (56)$$

$$= ab \frac{1}{\pi} \frac{\langle v^2 \rangle}{\tau} \int_{-\infty}^{\infty} \frac{1}{(\omega^2 + \frac{1}{\tau^2})(\omega^2 - \omega_o^2)} d\omega \quad (57)$$

$$= -ab \frac{\langle v^2 \rangle}{\omega_o^2} \frac{1}{\left(1 + \frac{1}{\omega_o^2 \tau^2}\right)} \quad (58)$$

This is in substantial agreement with the expression given in the caption of [2] Fig. 12 when it is taken with [2] Eq. (19) or (3) applicable to the case when $\omega_r \ll \omega_o$. It is quite likely that the small discrepancy ($\sim 10\%$) in the 50% suppression point is due to the process of averaging over the velocity distribution in [2] Fig. 12.

4.2 Diffusion theory calculation of the long time behavior of the velocity correlation function. Frequency shifts for $(\omega_r \gg \omega_o)$

Whereas the previous case applies to UCN this case would apply to atoms used as a comagnetometer and is more relevant experimentally as it results in larger shifts [2] and in some cases [9] the collision rate can be simply adjusted by changing the experimental conditions.

In the following we review the solution of the diffusion equation in cylindrical geometry, obtain the velocity autocorrelation function from the solution and calculate the frequency shift. In the limit of small collision rate the result agrees with the known results for $(\omega_r \gg \omega_o)$ and the effect of the collisions agrees with that found from numerical simulations ([2] Fig. 10)

4.2.1 Green's function for the diffusion equation in cylindrical geometry

In this section we attempt to understand the effects of the vessel boundary on the velocity autocorrelation function, observed in the numerical simulations (section 3.2), by applying classical diffusion theory to the problem. Diffusion theory is expected to be valid for long times so that we expect the results to be valid for small ω_o , i.e. $\omega_o \ll \omega_r$.

$$\begin{aligned} D\nabla^2\rho - \frac{\partial\rho}{\partial t} &= 0 \\ \rho &= u_k(r)e^{-Dk^2t} \\ \nabla^2u + k^2u &= 0 \end{aligned} \tag{59}$$

We consider a two dimensional problem, that is we neglect any z dependence ($k_z = 0$). For the cases considered in [2] where the height of the bottle is much smaller than the radius higher z modes will decay relatively quickly.

The boundary condition is $j(R) = -D\frac{\partial\rho}{\partial r} = 0$ so the eigenfunctions satisfying the boundary conditions are

$$\begin{aligned} u_{m,n} &= N_{m,n}J_m(k_{m,n}r)e^{im\theta} \\ k_{m,n}R &= x'_{m,n} \text{ (} n^{\text{th}} \text{ zero of } dJ_m(z)/dz \text{)} \end{aligned}$$

where the normalization constant (which depends on the boundary conditions) is ([10], p 322)

$$N_{m,n} = \frac{1}{\sqrt{2\pi}J_m(k_{m,n}R)} \sqrt{\frac{2k_{m,n}^2}{(k_{m,n}R)^2 - m^2}} \tag{60}$$

The Greens' function satisfying the boundary conditions is [16]

$$G(r, r', t) = \sum_{m,n} (N_{m,n})^2 J_m(k_{m,n}r) J_m(k_{m,n}r') e^{im(\theta-\theta')} e^{-Dk_{m,n}^2 t} \quad (61)$$

This is the probability of finding a particle at \vec{r} at time t , given that the particle was at \vec{r}' at time $t = 0$. The spectrum of the velocity correlation function is related to $S(\vec{q}, \omega)$ which in turn is the average over the system of the Fourier transform of this probability with respect to $\rho = (r - r')$. We use the cosine transform because we want the cosine transform of the velocity correlation function (49) $\psi(\omega)$.

$$S(q, \omega) = \frac{1}{\pi} \left\langle \int d^2\rho e^{i\vec{q}\cdot\vec{\rho}} \int_0^\infty dt \cos \omega t G(r, r', t) \right\rangle \quad (62)$$

$$= \frac{1}{\pi} \int \int \frac{d^2r'}{\pi R^2} d^2\rho e^{i\vec{q}\cdot\vec{\rho}} \int_0^\infty dt \cos \omega t G(r, r', t) \quad (63)$$

$$= \frac{1}{\pi^2 R^2} \sum_{m,n} (N_{m,n})^2 \int d^2r e^{i\vec{q}\cdot\vec{r}} J_m(k_{m,n}r) e^{im\theta} \times \quad (64)$$

$$\int d^2r' e^{-i\vec{q}\cdot\vec{r}'} J_m(k_{m,n}r') e^{-im\theta'} \frac{Dk_{m,n}^2}{\omega^2 + (Dk_{m,n}^2)^2} \quad (65)$$

Now we can evaluate the integrals using

$$J_m(x) = \frac{(-i)^m}{2\pi} \int_0^{2\pi} e^{i(x \cos \theta + m\theta)} d\theta \quad (66)$$

and Bessel function identities

$$\int d^2r e^{i\vec{q}\cdot\vec{r}} J_m(k_{m,n}r) e^{im\theta} = \frac{2\pi (i)^{\pm m}}{(q^2 - k_{m,n}^2)} \frac{qR}{2} J_m(k_{m,n}R) \times [J_{m-1}(qR) - J_{m+1}(qR)]$$

thus

$$S(q, \omega) = \frac{2}{\pi^3 R^2} \sum_{m,n} \dots \quad (67)$$

$$\frac{k_{m,n}^2}{((k_{m,n}R)^2 - m^2)} \left(\frac{2\pi}{(q^2 - k_{m,n}^2)} \frac{qR}{2} [J_{m-1}(qR) - J_{m+1}(qR)] \right)^2 \frac{Dk_{m,n}^2}{(\omega^2 + (Dk_{m,n}^2)^2)} \quad (68)$$

4.2.2 Velocity autocorrelation function

The velocity autocorrelation function

$$\psi(\tau) = \langle \vec{v}(0) \cdot \vec{v}(\tau) \rangle \quad (69)$$

has a Fourier transform given by ([11])

$$\psi(\omega) = \lim_{q \rightarrow 0} 2 \left(\frac{\omega}{q} \right)^2 S(q, \omega)$$

so that the only terms in (68) which contribute are those containing $J_0(qR)$, since $\lim_{x \rightarrow 0} J_n(x) \sim (x)^n$, $J_0(0) = 1$. Thus we only need to keep terms with $m = \pm 1$ in (68) and we find

$$\lim_{q \rightarrow 0} S(q, \omega) = \frac{4q^2}{\pi \left((k_{1,n}R)^2 - 1 \right)} \frac{D}{\left(\omega^2 + (Dk_{1,n}^2)^2 \right)} \quad (70)$$

Then

$$\psi(\omega) = \frac{1}{\pi} \sum_n \frac{8}{(x_{1,n}^2 - 1)} \frac{D\omega^2}{\left(\omega^2 + (Dk_{1,n}^2)^2 \right)} \quad (71)$$

4.2.3 Frequency shift in the diffusion approximation (cylindrical geometry)

According to (51)

$$\delta\omega = -ab \int_{-\infty}^{\infty} \psi(\omega) \frac{1}{\omega_o^2 - \omega^2} d\omega \quad (72)$$

$$= abR^2 \sum_n \frac{8}{(x_{1,n}^2 - 1)} \frac{1}{x_{1,n}^2 \left(\left(\frac{\omega_o R^2}{Dx_{1,n}^2} \right)^2 + 1 \right)} \quad (73)$$

The result (73) is dominated by the first mode $x_{1,1} = 1.84$. Figure 3 shows the first term in comparison to the sum of the first 4 terms. For convenience we list the zeroes of $J_1'(x)$: $x_{1,2} = 5.33$, $x_{1,3} = 8.54$, $x_{1,4} = 11.7$. Since we are dealing with a 2 dimensional problem we put

$$D = v^2\tau/2 \quad (74)$$

(instead of $\tau v^2/3$ for 3 dimensions) in order to facilitate the comparison with the numerical simulations [2] and obtain for the condition that the frequency shift is reduced to 50% of its value in the absence of collisions

$$\eta = \frac{\omega_o R^2}{D x_{1,n}^2} = \frac{2\omega_o R^2}{v^2 \tau x_{1,n}^2} = .59 \frac{\omega_o R^2}{v^2 \tau} = 1 \quad (75)$$

the numerical factor of which is to be compared with $\frac{2}{\pi} = .634$ obtained in JMP, fig. 10 by fitting simulated results, and our numerical result of 0.6 presented in Sec. 3.2. The magnitude abR^2 of (73) in the absence of collisions is just that expected from the Bloch-Siegert treatment in the case $\omega_r \gg \omega_o$ (equ. (3), [2] Eq. (21)).

4.2.4 Frequency shift in the diffusion approximation (rectangular geometry)

For the rectangular case the normalized eigenfunctions are

$$u_{m,n}(x, y) = \sqrt{\frac{2}{L_x}} \cos \frac{m\pi}{L_x} x \sqrt{\frac{2}{L_y}} \cos \frac{m\pi}{L_y} y \quad (76)$$

which satisfy the reflection boundary conditions at $x = 0, L_x$ and $y = 0, L_y$. For n or $m = 0$ the corresponding eigenfunctions are

$$u_0 = \frac{1}{\sqrt{L_{x,y}}} \quad (77)$$

so that the Green's function is

$$G(x, x', y, y', t) = \sum_{m,n=0}^{\infty} \left[\frac{1}{L_x} + \frac{2}{L_x} \cos k_m x \cos k_m x' e^{-Dk_m^2 t} \right] \times \left[\frac{1}{L_y} + \frac{2}{L_y} \cos k_n y \cos k_n y' e^{-Dk_n^2 t} \right] \quad (78)$$

with $k_{m,n} = (m, n) \pi / L_{x,y}$. To calculate $\lim_{q \rightarrow 0} S(q, \omega)$ we need integrals of the form

$$\lim_{q \rightarrow 0} \int_0^L e^{iq_x x} \cos k_m x dx = \frac{q_x}{q_x^2 - k_m^2} \left\{ \begin{array}{ll} q_x L_x & m = 2, 4, 6.. \\ \frac{-2}{i} & m = 1, 3, 5.. \end{array} \right\} \quad (79)$$

$$= \left\{ \begin{array}{ll} L_x & m = 0 \end{array} \right\} \quad (80)$$

Since each of these will appear squared because of the contribution from the x, x' integrals we can only take the odd values of m . The even numbers will

yield a higher power of q which will vanish in the limit. Given this, if we take $m = 1, 3, 5$ we must take $n = 0$ and vice-versa. We calculate, using (79)

$$\lim_{q \rightarrow 0} \left[S(q, \omega) = \int dx \int \frac{dx'}{L_x} \int dy \int \frac{dy'}{L_y} e^{i\vec{q} \cdot (\vec{x} - \vec{x}')} \frac{1}{\pi} \int_0^\infty dt \cos \omega t G(\vec{x}, \vec{x}', t) \right] \quad (81)$$

$$= q^2 \frac{8}{2\pi} \left(\sum_{m=1,3,5..} \frac{1}{k_m^2 (m\pi)^2} \frac{Dk_m^2}{\omega^2 + (Dk_m^2)^2} + \sum_{n=1,3,5..} \frac{1}{k_n^2 (n\pi)^2} \frac{Dk_n^2}{\omega^2 + (Dk_n^2)^2} \right) \quad (82)$$

where we used $\langle q_x^2 \rangle = \langle q_y^2 \rangle = q^2/2$. Then

$$\psi(\omega) = \frac{8\omega^2}{\pi} \left(\sum_{m=1,3,5..} \frac{1}{k_m^2 (m\pi)^2} \frac{Dk_m^2}{\omega^2 + (Dk_m^2)^2} + \sum_{n=1,3,5..} \frac{1}{k_n^2 (n\pi)^2} \frac{Dk_n^2}{\omega^2 + (Dk_n^2)^2} \right) \quad (83)$$

and (using 51)

$$\begin{aligned} \delta\omega &= -ab \int_{-\infty}^{\infty} \psi(\omega) \frac{1}{\omega_o^2 - \omega^2} d\omega \quad (84) \\ &= 8ab \left(\sum_{m=1,3,5..} \frac{L_x^2}{(m\pi)^4} \frac{1}{\left(\frac{\omega_o L_x^2}{D(m\pi)^2}\right)^2 + 1} + \sum_{n=1,3,5..} \frac{L_y^2}{(n\pi)^4} \frac{1}{\left(\frac{\omega_o L_y^2}{D(n\pi)^2}\right)^2 + 1} \right) \quad (85) \end{aligned}$$

We thus see that in a rectangular box $L_x \neq L_y$ it is the longer side which dominates the behavior.

4.3 Application: ^3He Comagnetometer

In [9] the use of ^3He as a comagnetometer for a UCN neutron EDM experiment is discussed. This system is rather unique in that an effective background gas (phonons) can be introduced which affects the ^3He significantly while having no substantial interaction with the UCN for temperatures below 0.5 K. Because the ^3He and neutron magnetic moments are equal to within 10%, it is possible to control this systematic by varying the size of the effect for ^3He by changing the diffusion rate of the ^3He .

The UCN upscattering lifetime varies as $100T^{-7}$ s for $T < 0.7$ K, while the coefficient of diffusion for ^3He in a superfluid helium bath varies as $D \approx 1.6T^{-7}$ cm²/s [17].

In connection with (75) this yields $\eta = 1$ when the superfluid helium temperature is $T \approx 0.25$ K, ($R=25\text{cm}$), which determines the temperature

scale where the effect can be varied, and is within the design range of operating temperature for the planned experiment, compatible with a UCN upscattering lifetime in excess of 1000 s.

5 Conclusion

We have developed a general analytic technique of analyzing the systematic effects due to a combination of an electric field and magnetic gradients as encountered in EDM experiments that employ gasses of stored particles. Use of the correlation technique, either by numerical calculations for complicated geometries, or by the velocity correlation function for simpler geometries, provides a simplified approach to the problem compared to numerical integration of the Bloch equations. Our analysis has added insight to this new systematic effect and provides a means of rapidly assessing the effects of various geometries.

6 Acknowledgements

We are grateful to Werner Heil and Yuri Sobolev for calling our attention to this problem and to George Jackeli and Boris Toperverg for an enlightening conversation. We also thank J.M. Pendlebury et al. for providing a draft of their manuscript before publication.

7 Appendix: Matrix algebra of spherical Pauli matrices

The following relationships among the Pauli matrices have been employed in the calculation in section 3.1.

$$2\sigma_{\pm} = \sigma_x \pm i\sigma_y \tag{86}$$

$$\sigma_{\pm}\sigma_z = \mp\sigma_{\pm}; \quad \sigma_z\sigma_{\pm} = \sigma_{\pm} \tag{87}$$

$$\sigma_{\pm}\sigma_{\mp} = \frac{1}{2} \pm \frac{1}{2}\sigma_z \tag{88}$$

$$\sigma_z\sigma_z = 1; \quad \sigma_{\pm}\sigma_{\pm} = 0 \tag{89}$$

References

- [1] Eugene D. Commins, Am. J. Phys. **59**, 1077 (1991).
- [2] J.M. Pendlebury et al., Phys Rev. A to be published (2004).
- [3] N.F. Ramsey, Phys. Rev. **100**, 1191 (1955).
- [4] D.D. McGregor, Phys. Rev. A **41**, 2631 (1990).
- [5] G.D. Cates, S.R. Schaefer, and W. Happer, Phys. Rev A **37**, 2877 (1988).
- [6] G.D. Cates et al., Phys. Rev A **38** (1988).
- [7] S.K. Lamoreaux, Phys. Rev. A **53**, R3705 (1996).
- [8] A. Abragam, *Principles of Nuclear Magnetism* (Clarendon Press, Oxford, 1961).
- [9] R. Golub and S.K Lamoreaux, Physics Reports **237**, 1-62 (1994).
- [10] A. Sommerfeld, *Partial Differential Equations* (New York, Academic Press, 1967).
- [11] This thorem, apparently based on work of DeGennes [12], has been cited by many authors, (e.g. [13,14,15]), with slightly different numerical constants. The most complete proof is given in [15]. The form we have used is appropriate for our two dimensional problem.
- [12] P.G. DeGennes, Physica **25**, 825 (1959)
- [13] Peter A. Egelstaff, *An introduction to the liquid state*, Academic Press, 1967
- [14] Stephen W. Lovesey, *Theory of neutron scattering from condensed matter, vol. 1* (Oxford : Clarendon Press ; New York : Oxford University Press, 1984).
- [15] G.L. Squires, *Introduction to the theory of Thermal Neutron Scattering*. Cambridge University Press, (1978)
- [16] Philip M. Morse and Herman Feshbach, *Methods of Theoretical Physics* (McGraw-Hill, New York, 1953), (Chapter 7).
- [17] S.K. Lamoreaux et al., Europhys. Lett. **58**, 718 (2002).

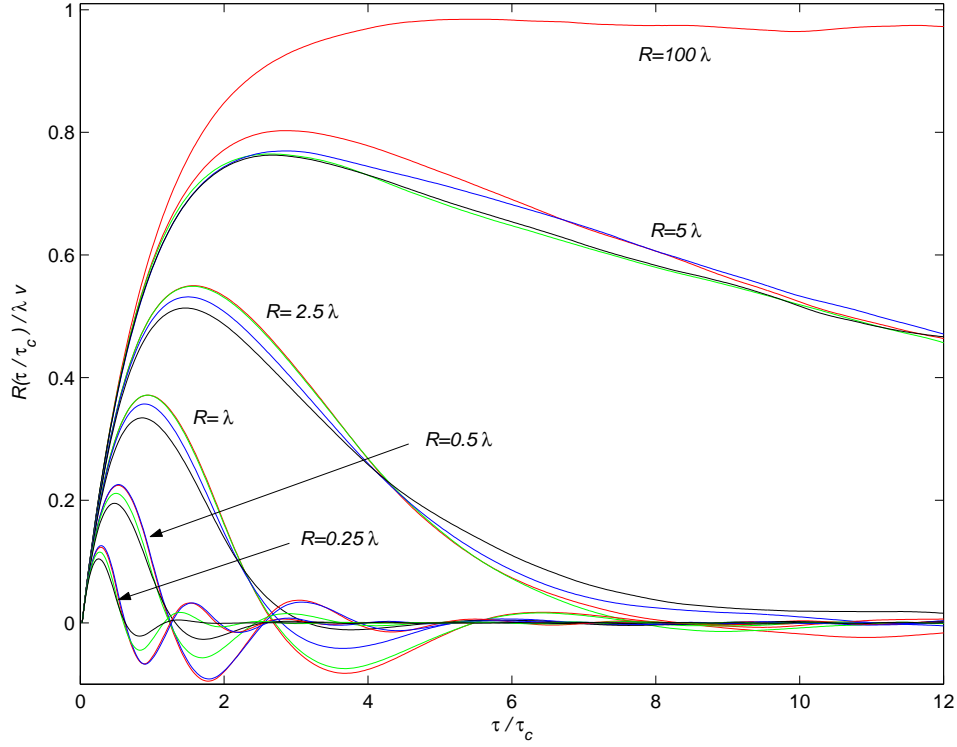


Figure 1: The position-velocity correlation function, $R(\tau) = 2h(\tau)$ as a function of cell radius R parameterized in terms of the mean free path λ for different degrees of specularly as parameterized by the angular spread of the final angle compared to the incident angle. Red: specular; Green: 45° ; Blue: 90° ; Black: diffuse. For $R \gtrsim 2.5\lambda$, there was practically no effect due to the degree of specularly, as expected.

8 Figures

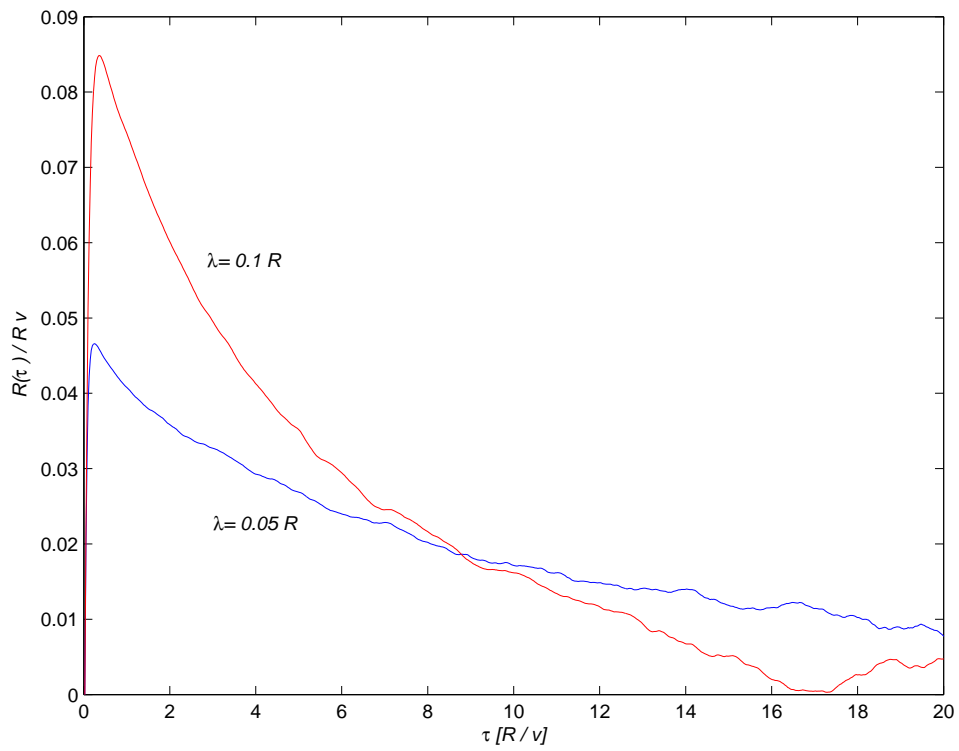


Figure 2: The position-velocity correlation function when λ is very small. This represents the limit for slow diffusion.

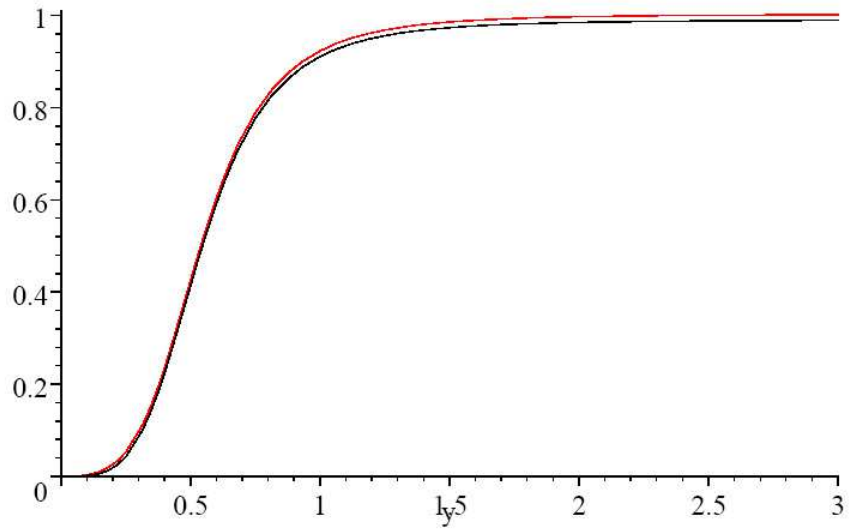


Figure 3: $\delta\omega/abR^2$ versus $y = \frac{D}{\omega_0 R^2}$ equation (73). Black first term, red sum of first 4 terms